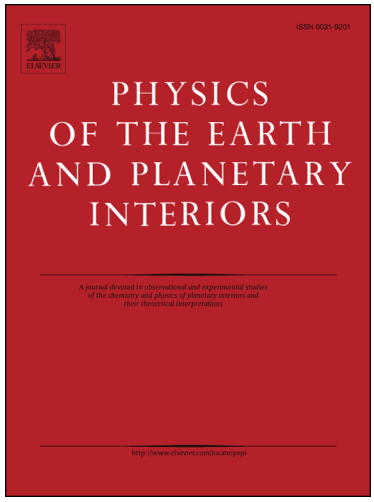

The carriers of AMS in remagnetized carbonates. Insights for remagnetization mechanism and basin evolution

Pablo Calvín, Juan J. Villalaín, Antonio M. Casas-Sainz

PII: S0031-9201(18)30063-3
DOI: https://doi.org/10.1016/j.pepi.2018.06.003
Reference: PEPI 6163

To appear in: *Physics of the Earth and Planetary Interiors*

Received Date: 5 March 2018
Revised Date: 12 June 2018
Accepted Date: 12 June 2018

Please cite this article as: Calvín, P., Villalaín, J.J., Casas-Sainz, A.M., The carriers of AMS in remagnetized carbonates. Insights for remagnetization mechanism and basin evolution, *Physics of the Earth and Planetary Interiors* (2018), doi: https://doi.org/10.1016/j.pepi.2018.06.003

The carriers of AMS in remagnetized carbonates. Insights for remagnetization mechanism and basin evolution.

Pablo Calvín[1,*], Juan J. Villalaín[1], Antonio M. Casas-Sainz[2]

[1]Departamento de Física, Universidad de Burgos. EPS Río Vena, Av. Cantabria s/n, 09001 Burgos (Spain). *Correspondence (calvinballester@gmail.com)

[2]Geotransfer Research Group (IUCA), Universidad de Zaragoza, C/ San Pedro Cerbuna 12, 50009 Zaragoza (Spain).

P.C. http://orcid.org/0000-0002-4485-213

J.V. http://orcid.org/0000-0001-9948-0953

A.C.S. http://orcid.org/0000-0003-3652-3527

Abstract

Magnetic fabrics are usually studied to unravel the evolution of sedimentary basins, mainly focusing the attention in paramagnetic minerals. However, since basins are sometimes affected by burial-related chemical remagnetizations, magnetic fabrics can also be carried by authigenic ferromagnetic minerals related to remagnetization processes. Consequently, the study of the different types of fabrics can give complementary and valuable information about the evolution of sedimentary basins. Here, we explore, in the Jurassic carbonates of the Central High Atlas (Morocco), the role in magnetic fabrics of authigenic magnetite that grew during the Cretaceous (*ca.* 100 Ma) widespread remagnetization event.

Magnetic fabrics are studied in 53 sites using the anisotropy of the magnetic susceptibility measured at room temperature (RT-AMS) and comparing results with sub-fabrics that alternatively enhance the paramagnetic and the ferromagnetic signal. Furthermore, an innovative analysis is proposed, comparing the magnetic fabrics before and after bedding correction (the common procedure) with fabric orientation after partial bedding correction. We use the paleomagnetic information to reconstruct the attitude of bedding at the remagnetization time and to restore the magnetic fabrics at this time.

The performed analysis allows interpreting RT-AMS in terms of the contribution of different subfabrics, and the relationship between these, tectonic processes and the magnetic mineralogy. Four RT-AMS types are defined: T1 is carried by superparamagnetic magnetite that grew during the remagnetization stage and shows a horizontal lineation parallel to the extension direction at this time; T3 and T4 are carried by paramagnetic minerals and show compressive fabrics with the magnetic lineation parallel to intersection (bedding-cleavage) lineation; finally, T2 shows a mix between ferrimagnetic and paramagnetic fabrics.

Keywords: magnetic fabrics, magnetic subfabrics, superparamagnetic fabric, limestone fabric, remagnetization, Central High Atlas.

INTRODUCTION

Since the first works by Graham (1954, 1966) evaluating the petrofabric of sedimentary rocks through the anisotropy of low field induced magnetization (i.e. the anisotropy of the magnetic susceptibility, AMS), this tool has been widely used to infer the petrofabric in a quick and reliable way (Borradaile and Tarling, 1981, Hrouda, 1982; Rochette and Vialon, 1984; Borradaile, 1988; Tarling and Hrouda, 1993; among others), even when other textural indicators are weakly developed. The measurement of AMS at room temperature (RT-AMS) gives the bulk information of the whole mineral assemblage in the rock (i.e. diamagnetic, paramagnetic and ferromagnetic s.l. minerals). Its application in phyllosilicate-rich sedimentary rocks lead to relatively straightforward inferences about the tectonic regime responsible for deformation in sedimentary units (see Parés 2004, 2015 for review). Therefore, AMS provides information about (i) the tectonic frame under which sediments were deposited and subsequently deformed (e.g. Aubourg et al., 2004, 2010; Borradaile and Hamilton, 2004; Caricchi et al., 2016; Cifelli et al., 2004, 2005; García-Lasanta et al., 2014, 2015; Kissel et al., 1986; Lee and Angelier, 2000; Mattei et al., 1997, 1999; Moussaid et al., 2013; Oliva-Urcia et al., 2009, 2011; Parés et al., 1999; Pueyo-Anchuela et al., 2011; Soto et al., 2009, 2012), (ii) subsequent tectonic imprints (e.g. Debacker et al., 2004; Dudzisz et al., 2018; Oliva-Urcia et al., 2013, 2018, Izquierdo-Llavall et al., 2013), or (iii) other common geological processes, such as the diapiric evolution both under compressional and extensional settings (Santolaria et al., 2015; Soto et al., 2017). This has led to refinement of evolutionary basin models and of fault activity during basin evolution.

However, a fundamental previous step before interpreting AMS is to determine the magnetic mineralogy that gives rise to the magnetic fabric, for a number of reasons: (i) different minerals can have a different origin and formation time; (ii) different minerals present different rheology and therefore their response to deformation can be variable; (iii) dia- para- and ferromagnetic s.l. fabrics can record and, therefore contribute, with different information, allowing a wider vision about the tectonic evolution experienced by rocks. There are different approaches that allow to assess which are the carriers of the RT-AMS, as for example: (i) sub-fabrics measurements, either by means of AMS measured at liquid nitrogen temperature (LT-AMS) (Richter and van der Pluijm, 1994; Parés and van der Pluijm, 2002, 2014; Issachar et al., 2016), through high-field and low-field measurements (e.g., Hrouda and Jelínek, 1990; Rochette and Fillion, 1988; Schmidt et al., 2007) or through the anisotropy of the remanence measured by different ways (e.g. McCabe et al., 1985; Jackson., 1991; Martín-Hernández and Ferré, 2007; Potter, 2004; Bilardello and Jackson, 2014); (ii) comparison between magnetic fabrics and petrographic observations (both under optical and electronic microscopes) or (iii) X-ray and neutron goniometry (e.g. Chadima et al., 2004; Martín-Hernández and Ferré, 2007; Cifelli et al., 2009; Schmidt et al., 2009; Oliva-Urcia et al., 2012). Usually the coincidence of axes orientations between RT-AMS and LT-AMS indicates that the carriers of the RT-AMS are paramagnetic minerals when the diamagnetic fabrics are excluded (or at least that the RT-AMS is equivalent to the paramagnetic petrofabric). Conversely, the coincidence in orientation between RT-AMS and anisotropy of the remanence indicates that the RT-AMS shows the petrofabric of the ferromagnetic s.l. minerals. It goes without saying that RT-AMS, LT-AMS and anisotropy of the remanence can all show similar orientations, thus indicating a coincidence between the petrofabric of paramagnetic and ferromagnetic minerals.

One of the first tests when working with magnetic fabric is to establish its relationship with bedding. The clustering degree between ellipsoids from different sites before and after bedding

correction is probably the quickest and most reliable way to determine this relationship. Paleomagnetic analysis provides a new element for comparing with the magnetic fabric: paleomagnetic directions of syn-folding remagnetizations allow to know the attitude of beds (i.e. the paleo-bedding) at the moment of remagnetization occurrence (e.g. Villalaín et al., 2003, 2016; Soto et al., 2008; Torres-López et al., 2015; García-Lasanta et al., 2017). Beyond the comparison before and after total bedding correction, it is possible to analyse the magnetic fabric after partial bedding correction (i.e. restoring strata to their paleo-bedding) and, in this way, to understand possible relationships between remagnetization and magnetic fabric acquisition.

Because of (i) the abundance of ferromagnetic fabrics, and the scarcity of phyllosilicates, and hence paramagnetic fabrics, in some rock types (namely marine limestones and dolostones), and (ii) the extent to which remagnetizations in sedimentary basins are found, the unravelling of the significance of the different types of magnetic fabrics in remagnetized rocks is of primary importance. This is especially significant if a thorough application of the AMS technique to sedimentary rocks is intended. In this work, we explore how the characteristic mineralogy of remagnetized limestones, containing significant amounts of superparamagnetic (SP) and stable single domain (SSD) magnetite (e.g. Jackson and Swanson-Hysell, 2012, for review) affects the RT-AMS. For that purpose, on one hand (i) magnetic sub-fabrics (LT-AMS and anisotropy of the anhysteretic remanent magnetization -AARM) are compared with RT-AMS, and on the other hand, (ii) we propose the complementary test of comparing the magnetic fabric with the paleo-bedding in addition to the usual comparison with bedding, to understand the timing of acquisition of the RT-AMS. The results obtained are of interest for the study of other marine and non-marine sedimentary basins and widens the range of applicability of AMS as a reliable marker in basin analysis.

GEOLOGICAL SETTING

The Atlas system is an ENE-WSW intracontinental chain located in the foreland of the southernmost sector of the Mediterranean Alpine System, in NW Africa (Fig. 1a). The chain is the result of the Cenozoic convergence between African and European plates, which generated the inversion of a system of Mesozoic extensional basins (Mattauer et al., 1977; Gomez et al., 2000; Frizon de Lamotte et al., 2008).

Because of its intrinsic geological and paleomagnetic features, the Central High Atlas (CHA; Fig. 1b) provides an outstanding location for the study of AMS linked to remagnetized limestones because of (i) the widespread remagnetization that involves 80% of the width of the mountain chain and extends at least from the Atlantic coast to the Saharan Atlas, affecting different types of rocks and (ii) the thickness and lithological variety of the Jurassic calcareous sequences. The tectonic evolution of the High Atlas and the stress directions at each stage are relatively well known (e.g. Ait-Brahim et al., 2002) and magnetic properties of limestones have also been the target of several paleomagnetic works (Torres-López et al., 2014, 2016; Calvín et al., 2017a). Mesozoic extension, especially during the Triassic and the Jurassic (Fig. 2), was responsible for (i) the deposition of several thousand meters of red beds and marine limestones in overall, and (ii) a complex thermal history that included the deposition of intercalated lava flows and the intrusion of basic rocks in several episodes (Hailwood and Mitchel, 1971; Armando, 1999; Haddoumi et al., 2002; Zayane et al., 2002; Bensalah et al., 2013; Calvín et al., 2017b and references therein), including gabbroic bodies and dyke complexes. Furthermore, the basinal stage, and also probably the inversion stage, were characterized by diapiric processes, favoured by the presence of a thick evaporitic unit at the bottom of the Jurassic sequence and triggered by tectonic movements and igneous activity (Michard et al., 2011; Torres-López et al., 2016). Structures formed as a consequence of salt tectonics, and triggered by regional deformation developed at one time with folds, thrusts and alternatively normal faulting.

The Mesozoic extensional stage is related to the opening of the Central Atlantic (especially in the western part of the Atlasic realm) and the evolution of the Western Tethys (Oliva-Urcia et al., 2016). Orientations of stress axes during the Mesozoic and Cenozoic in the Moroccan High-Atlas are relatively well established: WNW-ESE extension in Triassic times was succeeded by NW-SE extension, at least until Middle Jurassic times. From this time onwards, sedimentation rate dramatically diminished and other indicators, such as magmatic products, must be used to understand the tectonic frame. Late Jurassic to Early Cretaceous dykes provide a N-S extension direction, and probably re-used older structures (Ait-Brahim et al., 2002). N-S compression prevailed during the Eocene (with a previous weaker episode of E-W shortening) to finally change to a NW-SE direction in recent times (Fig. 2).

THE *ca.* 100 MA REMAGNETIZATION IN THE CENTRAL HIGH ATLAS

Previous paleomagnetic studies carried out in the CHA (e.g. Torres-López et al., 2014; Moussaid et al., 2015; Calvín et al., 2018) divide the Mesozoic deformational history in three main stages: pre, syn and post *ca.* 100 Ma remagnetization (Fig. 2). This remagnetization has an inter-folding behaviour (Fig. 2) because it was acquired between two deformational stages (the Mesozoic extension and the Cenozoic compression), both responsible for the ENE-WSW structure of the CHA.

From the analysis of the paleomagnetic vectors after the calculation of the remagnetization direction, it is possible to make a restoration of the attitude of beds at *ca.* 100 Ma (Torres-López et al., 2016; Villalaín et al., 2016; Calvín et al., 2017c). The AMS sites studied in this work were previously analysed paleomagnetically by Calvín et al. (2017a) and therefore we can use the paleo-dip (i.e. the *ca.* 100 Ma bedding orientation) to restore the magnetic fabrics at the remagnetization acquisition moment. Then, three orientations of AMS can be compared: before bedding correction (BBC), after partial

bedding correction (APBC, i.e. restoring at the paleo-dip) and after total bedding correction (ATBP, i.e. restoring the bedding at the horizontal).

Another important point when analysing the magnetic fabrics in remagnetized limestones is their specific magnetic mineralogy. Chemical remagnetizations carried by magnetite are characterized by large amounts of superparamagnetic (SP) and stable single domain (SSD) grains (see Jackson and Swanson-Hysell, 2012 for review) that show shape anisotropy (Calvín et al., submitted). Comparing the AARM in the three stages, Calvín et al. (submitted) observed that the ferrimagnetic fabric of the limestones in the CHA is carried by the diagenetic magnetite responsible for the Cretaceous remagnetization. This fabric shows the best cluster APBC, with a horizontal cluster of the magnetic lineation in a NNE-SSW direction, which is interpreted as the extension direction at the remagnetization time.

APPLIED TECHNIQUES

The magnetic fabric of cylindrical standard specimens was assessed by means of three techniques: anisotropy of the magnetic susceptibility measured at room and low temperature (liquid nitrogen temperature; ~ 77 K) (RT-AMS and LT-AMS respectively) and through the anisotropy of the anhysteretic remanent remagnetization (AARM). RT-AMS is an approximation to the petrofabric of the rock in which all minerals contribute to the bulk signal (diamagnetic, paramagnetic and ferromagnetic s.l. minerals). LT-AMS amplifies the paramagnetic contribution to the AMS signature (Richter and van der Pluijm, 1994; Parés and van der Pluijm, 2002) according to the Curie-Weiss law (the paramagnetic susceptibility at 77 K is 3.8 times greater than at room temperature). Finally, AARM (McCabe et al., 1984) indicates the magnetic anisotropy of ferromagnetic s.l. grains with coercivities in the range between 0 and 90 mT, i.e., mainly ferrimagnetic minerals.

The AMS is a symmetric, second rank tensor, whose eigenvalues and eigenvectors can be used to define an ellipsoid with orthogonal principal axes, $k_{max} > k_{int} > k_{min}$. The shape and the anisotropy degree defined by the ellipsoid are determined using the T and Pj parameters (Jelinek, 1981) respectively, and the bulk susceptibility is defined by $k_m = [(k_{max} + k_{int} + k_{min}) / 3]$ (Nagata, 1961). AMS experiments were carried out with a KLY4-S Kappabridge (AGICO) (875 Hz and 300 A/m). For measurements at low temperature (LT-AMS), specimens were submerged into liquid nitrogen about 45 min before starting the experiments, and 10-15 min between measurements.

The AARM was measured in 17 specimens from four sites (four to five specimens per site) and were evaluated together with previous AARM results from the same sites (presented in Calvín et al., 2018), totalling 63 specimens from 13 sites. The procedure for AARM analysis consists in the measurement of nine different positions of the sample, previously demagnetized, after the acquisition of an anhysteretic field along the axis of measurement (see McCabe et al., 1984). The magnetic second-rank tensor is calculated following Girdler's (1961) procedure. AARM measurements were made with a 2G cryogenic magnetometer with integrated alternating field (AF) and direct field (DF) coils. We used a DF of 0.05 mT imparted coaxially with an AF between 90 and 0 mT. Anhysteretic magnetization was demagnetized after each measurement in a peak alternating field of 100 mT and this measurement was used as a baseline to each position to remove the contribution of higher coercivity minerals.

The studied sites have been previously analysed paleomagnetically (Calvín et al., 2017a), giving information about the paleo-dip of bedding at the age of remagnetization (*ca.* 100 Ma). This information allows applying a double restoration to the magnetic ellipsoid. In addition to the magnetic ellipsoid before bedding correction (BBC; i.e. in situ), we can analyse it after partial bedding correction (APBC; i.e. after untilting the beds to their *ca.* 100 Ma attitude) and after total bedding correction (ATBC; i.e. after restoring the bedding to the horizontal). In this way, we can observe the coherence at the different evolutionary stages.

In addition, several rock-magnetic experiments were made in order to understand the link between the magnetic minerals present in the specimens and the magnetic fabrics. Temperature-dependent susceptibility curves were carried out using a KLY4 Kappabridge (AGICO) with a CS3 furnace (temperature range between 25 and 700 ºC) and a CSL cryostat (from -195 to 0 ºC) under argon atmosphere. The variation of the bulk susceptibility with the frequency, expressed as the percentage of frequency-dependent susceptibility parameter (% χfd; Dearing et al., 1996), was used to assess the contribution of the superparamagnetic fraction to the bulk susceptibility.

LITHOLOGICAL AND TEXTURAL CHARACTERIZATION

The present day ENE-WSW structure of the CHA (Fig. 3) is the consequence of the mainly NW-SE directed extension that generated ENE-WSW basins during the Mesozoic (especially during the Jurassic) and the subsequent N-S Cenozoic compression (e.g. Frizon de Lamotte et al., 2008). The study area presents a particular deformation style (Fig. 1c) that is strongly conditioned by (i) the thick sedimentary sequences and (ii) the inherited extensional geometry, consisting of wide, flat areas separated by antiforms related to halokinetic and igneous activity, many of them already configured at the remagnetization time (Torres-López et al., 2016) (Fig. 3c).

These structures were reactivated under compression, and the antiforms were squeezed and thrusted during the Cenozoic, accommodating part of the deformation. The areas between antiforms are folded, generally by angular folds, and show development of axial-plane cleavage (Calvín et al., 2017a) (Figs. 3d and 4). At outcrop scale (Fig. 4) this cleavage appears as fracture (e.g. AM01) or pressure-solution (e.g. SK05) cleavage with different degrees of development depending on the lithology involved and its location within the basin, ranging from nodular limestones without evidence of cleavage (e.g. DP01) to moderate (e.g., AM06, AM08, SK14) and penetrative cleavage (e.g. SK01, AM09) that can obliterate the bedding to some extent (e.g. OU01). Pencil structures (e.g. AM01) can

be observed in some outcrops and the bedding-cleavage angle is variable, ranging from almost perpendicular (e.g. SK05) to sub-parallel (e.g. SK14).

Observations under the petrographical microscope (Fig. 5) also show a variety of features concerning both lithology and deformation degree, which is not always evident at outcrop scale. One common feature of all observed samples is the presence of bedding-parallel, platy pyrite grains or laminae, often formed by aggregates of crystals with cubic or framboidal shape. Many of these grains probably have been partially altered to magnetite during the remagnetization process. AG02 is a bioclastic limestone without cleavage and presenting stratiform stylolites. SK14, SK05 and AM01 are micritic limestones with some contribution of detrital grains (quartz and phyllosilicates) showing different degrees of cleavage development. In these samples the bedding is defined by oriented phyllosilicates and subtle changes in grain size. Cleavage is defined by faint pressure-solution surfaces and grain orientation in SK14, better defined in SK05 by the accumulation of opaque minerals. SK01 shows the better-defined solution surfaces with accumulation of opaque minerals; probably most of the opaque minerals correspond to iron oxides, but also to very fine-grained shales that can be present in all samples although individual minerals are not visible at this scale.

AMS RESULTS (RT-AMS, LT-AMS, AARM)

Measured specimens show a mean low-field susceptibility (κ) at room temperature (RT-AMS) of 234 $x10^{-6}$ SI (σ = 245 $x10^{-6}$ SI), with a range of 37 $x10^{-6}$ SI and 1596 $x10^{-6}$ SI (Fig. 6a). The anisotropy degree reflected by the Pj parameter has a mean of 1.027 (σ = 0.016) ranging between 1.004 and 1.099. Finally, the shape parameter T is variable, with a mean value of -0.008 (σ = 0.461), with a range of -0.959 and 0.917 (Fig. 5; Table 1) indicating similar number of samples with prolate and oblate ellipsoids. LT-AMS (Fig. 6b) shows similar parameters, with the exception of the T parameter, showing

mainly oblate ellipsoids (positive T values), contrasting with AARM, which shows prolate ellipsoids (negative T values).

A visual inspection of the principal axes of the RT-AMS of the set of 53 measured sites (Fig. 6a) shows a roughly horizontal foliation. This is better defined (confidence angles are lower) both APBC and ATBC rather than BBC. The maximum axis k_{max} is scattered in the horizontal plane (preferably APBC and ATBC). However, none of the projections shows a clean, clustered distribution of the RT-AMS axes, probably due to a mix of different magnetic fabrics.

Sub-fabrics determined from LT-AMS (enhanced paramagnetic fabric) and the AARM (ferrimagnetic fabric), although defined from a lower number of samples, are in general better clustered than the RT-AMS (Fig. 6b, c). LT-AMS is more scattered BBC and APBC compared to ATBC, which shows a horizontal magnetic foliation (indicating a sedimentary origin for most of the paramagnetic foliation) and a scattered ESE-WNW horizontal magnetic lineation. Nevertheless, in AARM the best clustering is APBC, indicating that the ferrimagnetic fabric was acquired coeval with the remagnetization (Calvín et al., submitted).

A site-by-site detailed comparison of the different sub-fabrics (Figs. 7 and 8) allows differentiating four different types of RT-AMS, according to the geometry and orientation of the magnetic ellipsoids and the distribution of their axes. Forty-four out of the 53 sites are included in one or another of these groups, whereas nine sites cannot be classified because of the dispersion of AMS axes at site scale or their anomalous orientation with respect to the deformation axes (labelled as 'unclassified' at Table 2).

Type 1 RT-AMS (Fig. 7a) is defined by a well clustered NNW-SSW lineation that becomes horizontal APBC, and a girdle between k_{min} and k_{int}, with a dominantly vertical k_{min}. The RT-AMS fabric is similar to the ferromagnetic fabric defined by the AARM. The prolate geometry of both

ellipsoids is also consistent with the prolate behaviour at specimen level (negative values of T parameter). The opposite happens when the paramagnetic fabric is enhanced through the LT-AMS: the mean, as well as the specimen ellipsoids, become triaxial (positive values of T parameter); the orientation of the principal axes is almost equal to RT-AMS, but the magnetic foliation becomes horizontal ATBC instead of APBC. Although this difference is subtle for low paleo-dips, it is significant because this is one of the major differential facts between fabric types 1 and 2.

Type 2 RT-AMS (Fig. 7b) is characterized by a triaxial to oblate ellipsoid, with a well-defined magnetic foliation. RT-AMS foliation is coincident with LT-AMS but slightly different from AARM, which shows more dispersion of k_{min}. Besides, in both magnetic susceptibility fabrics, magnetic foliation is horizontal ATBC whereas in the AARM this happens in the APBC orientation. Regarding the lineation, it is noteworthy that k_{max} at LT-AMS progressively approaches the intersection lineation between bedding and cleavage (L_1). Conversely, k_{max} for RT-AMS and AARM ellipsoids tends to be parallel to the general NNW-SSW trend observed in type 1 fabrics (Fig. 7a).

Type 3 RT-AMS (Fig. 8a) is defined by the coincidence between k_{max} and L_1, but keeping the magnetic foliation parallel to the bedding. LT-AMS behaviour is similar to RT-AMS and both show triaxial ellipsoids. Conversely AARM is similar to type1; the axes show a girdle between k_{max} and k_{int} (thus forming a prolate ellipsoid); however, at specimen level this difference is not evident, since triaxial to oblate behaviour was observed in most samples with independence of the type of sub-fabric.

Finally, type 4 RT-AMS (Fig. 8b) is clearly related to cleavage, showing oblate ellipsoids with k_{max} parallel to L_1, and a clustered k_{min} perpendicular to cleavage planes, both in RT- and LT-AMS. As in type 3, AARM does not show evidence for being affected by the tectonic cleavage, showing the same behaviour to that observed in type 1. In this case, differences can be observed at specimen level, showing oblate ellipsoids in AMS (with higher anisotropy in LT-AMS) and prolate ellipsoids in AARM.

These observations are enhanced in the projection of the RT-AMS of all sites classified by behaviour types (Fig. 9). Types 1 and 2 are similar, but magnetic lineation is better defined in type 1 (Fig. 9a) and magnetic foliation in type 2 (Fig. 9b), in agreement with the existence of more prolate specimens ($T < 1$) for type 1 and oblate ones ($T > 1$) for type 2. The best clustering in type 1 takes place APBC whereas in type 2 this arrangement is met ATBC, with vertical k_{min} and k_{max} oriented NNE-SSW. On the other hand, type 3 (Fig. 9c) shows the best clustering ATBC and the more scattered distribution BBC, as in type 2. However, the magnetic lineation is roughly NE-SW, parallel to the NE-SW regional trend of compressional structures. Type 4 (Fig. 9d) does not show a good clustering for any of the bedding corrections. At site level (Table 2) k_{min} is normal to cleavage and k_{max} is parallel to L_1. Finally, the 9 sites showing unclassified behaviour (Fig. 9e) are characterized mainly by strong dispersion at site level. A dominant NW-SE trend for the magnetic lineation can be observed before any correction in these sites.

ORIGIN OF THE DIFFERENT RT-AMS TYPES AND IMPLICATIONS

Magnetic mineralogy

The correspondence between the RT-AMS and the sub-fabrics indicates that the magnetic mineralogy (together with the deformation degree) is one of the principal factors that control the different types of RT-AMS observed. Whereas the ferrimagnetic fabric expressed by the AARM is always of type 1, the enhanced paramagnetic fabric (LT-AMS) tends to fit types 3 and 4. The ratio between the bulk susceptibility measured at low and room temperature (κ_{LT}/κ_{RT}; Fig. 10a) is in agreement with directional observations: ratios between 1 and 2 (presumably indicating a minor contribution of paramagnetic minerals) are typical of type 1 fabrics, ratios around 2 are mostly found in type 2 and ratios between 2 and 4 are found in types 3 and 4. Besides, comparing this ratio with κ_{RT}

(Fig. 10a), we find a correspondence between 'ferromagnetic' κ_{LT}/κ_{RT} ratios (lower than 2) and high κ_{RT} values, indicating that samples with predominance of paramagnetic phases present κ_{RT} values up to 250 x 10^{-6} SI, and higher κ_{RT} values indicate dominance of ferromagnetic phases.

Susceptibility-temperature (κ-T) heating curves (Fig. 10b) for type 1 fabrics show a major contribution of ferromagnetic s.l. minerals, with a progressive decay of the susceptibility during heating without following the typical hyperbolic behaviour indicated by the Curie-Weiss law of paramagnetic minerals. According to previous paleomagnetic works in these rocks (Torres-López et al., 2014; Calvín et al., 2017a), the main ferromagnetic phase is magnetite, with a dominance of the superparamagnetic (SP) and stable single domain (SSD) states. Although not so clearly, AM13-07 sample shows a sharp fall between 500-600 ºC. It is noteworthy the main decay at low temperature (between -200 and -150 ºC) in type 1 samples that is not present in the other types. This decay could correspond with the Verwey transition (Verwey, 1939; Walz, 2002) or could be related to the presence of SP magnetite (Worm, 1998; Worm and Jackson, 1999; Zhao and Liu, 2010) or titanomagnetite (Radhakrishnamurty and Likhite, 1993; Moskowitz et al., 1998); absence of clear Verwey transitions in samples with dominance of magnetite can be explained if the magnetite is not perfectly stoichiometric or if it is partially oxidized (e.g., Özemir et al., 1993). On the other hand, paramagnetic phases dominate κ-T curves in types 2, 3, and 4, with hyperbolic shapes of the curves. Between 400 and 600 ºC, susceptibility increases and falls again due to neoformation of ferromagnetic minerals. In all cases, neoformation of different ferromagnetic phases is important, resulting in irreversible curves (cooling curves show evident increase of the susceptibility), as in AM04-09. These neoformed ferromagnetic phases have Curie temperatures between 450 and 600 ºC, probably indicating the formation of non-stoichiometric magnetite.

Site AM13 (Fig. 10c) shows a mixed of behaviour between types 1 and 2 in correspondence with the κ-T curves. Specimens AM13-03 and AM13-04 of this site show a dominant paramagnetic

behaviour in κ-T curves and type 2 RT-AMS behaviour, with an oblate ellipsoid and k_{min} becoming vertical ATBC. Conversely, ferromagnetic phases are dominant in AM13-07 and, as the rest of specimens, it shows a prolate ellipsoid whose k_{max} becomes horizontal APBC, indicating a type 1 RT-AMS. It is noteworthy that k_{max} shows similar orientations in all the above-described specimens and differences only arise in the orientation of the magnetic foliation. The results obtained for AM13 site are similar to the example illustrated in site AM06 (Fig. 7b), which shows in an overall view a type 2 behaviour. However, whereas k_{min} axes of RT- and LT-AMS are equal, k_{max} axes are different; in this case, k_{max} axes of RT-AMS are similar to the ones representing the AARM. This can be interpreted as a superposed magnetic fabric in the RT-AMS, in which magnetic foliation is defined by paramagnetic minerals and magnetic lineation by ferromagnetic s.l. minerals.

Figure 11 illustrates different magnetic properties of samples for the defined RT-AMS types. The ratios between the hysteresis parameters (Day plot; Fig. 10a) show dispersion along the SP-SSD mixing curves, typical of remagnetized limestones (Channel and McCabe, 1994; Jackson and Swanson-Hysell, 2012), without differences between samples belonging to the different groups. This behaviour discards mineralogical grain-size differences of magnetite between fabric types.

ARM susceptibility (χ_{ARM}; Fig. 11b) in remagnetized limestones is indicative of the amount of SSD magnetite. Despite of the overlapping present in the box and whisker plots, type 1 shows higher values than the others. κ_{RT} (Fig. 11c) does not show major differences despite the observations made comparing the κ_{LT}/κ_{RT} vs. κ_{RT} plot (Fig. 10a), where types 2, 3 and 4 showed similar κ_{RT} values (between 50 and 300 x 10^{-6} SI) while type 1 specimens showed higher values (note the difference of measured samples between both plots). It is interesting to compare the percentage of variation in the susceptibility measured at low (470 Hz) and high frequencies (4700 Hz) ($\%\chi_{fd}$; Fig. 11d). This ratio is indicative of the contribution of SP grains to the bulk susceptibility. Type 1 specimens show high ratios (median of 9 $\%\chi_{fd}$), indicating a strong contribution from SP grains, whereas the other types show

medians around 5 and 7 $\%\chi_{fd}$, indicating mixing of SP and non-SP contributions to the bulk susceptibility. Finally, a comparison of the shape parameter T (Fig. 11e) both of the RT-AMS and the AARM between different types show dominantly negative values (prolate ellipsoid) of AARM in all types except for type 2, whereas T values for the RT-AMS are mostly positive with the exception of type 1. Therefore, T values are similar both for AARM and RT-AMS in types 1 and 2 (although dominantly negative in the first case and positive in the second) and conversely, types 3 and 4 show different behaviour, and therefore different carriers, between AARM and RT-AMS.

It is remarkable the fact that inverse fabrics (Stephenson et al., 1986; Potter and Stephenson, 1988; Rochette et al., 1992) are mostly absent. The presence of this kind of fabric could be a priori expected due to (i) the high contribution of ferrimagnetic grains to the overall susceptibility (especially in type 1) and (ii) the uniaxial anisotropy of the SSD magnetites present in these rocks (Calvín et al., submitted). However, in addition to SSD magnetite grains, remagnetized limestones show a high amount of SP magnetite (Jackson and Swanson-Hysell, 2012), which presents higher values of susceptibility than SSD, especially in the SP-SSD threshold (Worm, 1998; Hrouda and Ježek, 2014; Lanci and Zanella, 2016). A similar tendency in the χ_{ARM} and the $\%\chi_{fd}$ (Fig. 10) indicates a direct relation between the amount of SSD and SP magnetite (indicative for the first and the second parameters respectively). Furthermore, SSD and SP magnetic fabrics should have ellipsoids with equal orientation but with an interchange of the principal axes. The sum of the two ellipsoids results in an increase of the isotropy of the observed ellipsoid but without modification of its orientation (Ferré, 2002). All of this can explain the absence of inverse magnetic fabrics in RT-AMS or deviation in the orientation of the principal axes because specimens with high contribution of SSD also present high contribution of SP grains, which are dominant in the bulk susceptibility and without the capability of showing inverse fabrics.

Although most of these parameters allow separating type 1 (ferrimagnetic RT-AMS), type 2 (combined RT-AMS) and types 3 and 4 (paramagnetic RT-AMS), there is overlapping of the different indicators between the defined groups (e.g. in the κ_{LT}/κ_{RT} ratios, the χARM or the $\%\chi_{fd}$). This can be explained in two non-exclusionary ways. (i) These parameters measure the bulk contribution to the susceptibility without considering the anisotropy of the carriers of the susceptibility. As an example, samples without phyllosilicates but containing large amounts of pyrite (both are paramagnetic minerals) and a minor contribution of magnetite to the bulk susceptibility, can show a paramagnetic behaviour according to the bulk parameters. This can occur at the same time that the RT-AMS is carried by the magnetite grains if magnetite is more anisotropic than pyrite. (ii) The second explanation, exemplified by site AM13, is the heterogeneity within sites. The types of RT-AMS have been defined observing the directional behaviour at site level and differences between specimens can exist even if they are not obvious.

In any case, it seems evident that in type 1 the ferrimagnetic phases are dominant, showing low $\kappa_{LT}/\ \kappa_{RT}$ ratios (mostly between 1 and 2), ferromagnetic-shaped κ-T curves, and an important contribution of SP grains. Conversely, types 3 and 4 show that the paramagnetic phases are dominant, with $\kappa_{LT}/\ \kappa_{RT}$ ratios between 2 and 4 and hyperbolic κ-T curves. Type 2 shows intermediate behaviour, but with a dominance of the paramagnetic phases in κ-T curves.

Tectonic meaning of AMS in relation to basin evolution

A summary of the main geological processes probably having an imprint on the magnetic fabrics are the following: (i) sedimentation of carbonates during the Jurassic in a NW-SE extensional setting; (ii) syn-sedimentary deformation due to extensional tectonics and subsequent diapirism generating paleo-dips; (iii) *ca.* 100 Ma widespread chemical remagnetization due to the neoformation

of SP and SSD magnetite grains; (iv) Cenozoic N-S compression developing folding and regional cleavage.

According to observations in other extensional basins (e.g., Cifelli et al., 2005; García-Lasanta et al., 2014), phyllosilicates usually define a RT-AMS characterized by horizontal k_{max} axes perpendicular to the strike of normal faults and parallel to the stretching direction and k_{min} axes perpendicular to bedding. On the other hand, Calvín et al. (submitted) observed in the same rocks involved in this study, that the AARM defines a horizontal NW-SE magnetic lineation and its k_{min} is vertical defining a girdle together with k_{int}; this AARM is considered to be carried by the authigenic grains that grew during the *ca.* 100 Ma chemical remagnetization process, and aligning according to the general extension direction during this stage. Several works (Sagnotti et al., 1998; Parés, 2004; Pueyo-Anchuela et al., 2010; Dudzisz et al., 2018, among others) have indicated a relationship between phyllosilicate-related RT-AMS and compression in weakly deformed rocks, with the development of a RT-AMS defined by k_{max} parallel to the strike of compressional structures and to the intersection lineation, keeping their k_{min} perpendicular to bedding. The increase of flattening develops a transition to tectonic magnetic fabrics in which k_{min} becomes perpendicular to cleavage planes.

Similar extensional and compressional directional features can be observed in the different types of RT-AMS described in this work (Fig. 12). Type 1 fabric is carried by mostly ferrimagnetic grains that also carry the AARM, corresponding to the authigenic grains of magnetite related to remagnetization. As discussed in the previous subsection, the orientation of the principal axes in the RT-AMS reflects the orientation of SP instead SSD magnetite grains, because of the absence of generalized inverse fabrics Since the growth of the SP and SSD is coeval, they show the same orientation despite differences in size, and the contribution of SSD grains should be limited to the increase in the isotropy of the resultant ellipsoid (Ferré, 2002). In any case, type 1 fabric reflects the extension direction during the remagnetization time.

RT-AMS types 3 and 4 have a good correspondence with compressional fabrics carried by phyllosilicates. Type 3 is indicative of lower degree of deformation, with the k_{min} still normal to bedding (and therefore compaction-related), and the k_{max} parallel to the intersection lineation, whereas type 4 shows the same relation between k_{max} and the intersection lineation, but the k_{min} is normal to cleavage.

Finally, the case of type 2 is more difficult to analyse. In first instance, it is possible to consider this RT-AMS type as carried by phyllosilicates and defining an extensional fabric, with its k_{min} axis perpendicular to bedding and the k_{max} parallel to the Jurassic stretching direction at the basinal scale. However, the analysed parameters indicate an intermediate behaviour between paramagnetic and ferromagnetic minerals. Besides, when LT-AMS is available, its k_{min} is coincident with RT-AMS but not its k_{max}. LT-AMS shows the magnetic lineation parallel to the intersection lineation L_1, being coincident the lineations of RT-AMS and AARM. This can be interpreted as a mix between types 1 and 3: the more prolate ferrimagnetic fabric defines the lineation and the more oblate paramagnetic fabric defines the foliation. Since there are not LT-AMS data for all sites classified as type 2, the presence of some kind of extensional fabrics within this type cannot be excluded. In any case, most sites with paramagnetic fabric only present compressional RT-AMS, indicating that possible paramagnetic extensional fabrics in this area were overprinted during the Cenozoic compression.

The behaviour of the authigenic magnetite grains under deformation

The analysed samples do not show syn-compressional RT-AMS fabrics of ferrimagnetic origin (Fig. 11). Site AM08 shows how the ferrimagnetic fabric (by means of the AARM in this site) preserves the original extensional fabric in spite of the well developed pressure-solution cleavage in this site, which leads to define a type 4 RT-AMS carried by phyllosilicates, that reflects the compression. This fact implies that phyllosilicates and magnetite are not related. The growth of magnetite grains during

remagnetizations can be related to smectite-illite transformations associated with the increase in temperature during burial and the generation of magnetite during the diagenetic process (McCabe and Elmore, 1989; Katz et al., 1998) and/or with oxidation of pyrite during burial (Suk et al., 1990; Banerjee et al., 1997). Since phyllosilicates and magnetite define very different magnetic fabrics, authigenic magnetite did not grow mimetically with phyllosilicates and this could indicate that the smectite-illite transformation is not the process (or at least not the main process) that triggers the remagnetization. Conversely, the oxidation of pyrite can explain our observations in the different magnetic sub-fabrics and therefore this could correspond with the remagnetization mechanism in the studied carbonates. The isotropic shape of pyrite grains does not seem to be affected by flattening, if small grains of magnetite (nanometre grains) grew inside the pyrite grains as external rims (this has been observed in several remagnetized rocks; e.g., Suk, 1993; Blumstein et al., 2004; Oliva-Urcia et al., 2009; Kars et al., 2014), non-deformed pyrite grains could have prevented deformation of magnetite grains, as well. Following this line of logic, pyrite grains provide an isotropic medium in which magnetite grains can grow without following previous sedimentary or tectonic structures (e.g. sedimentary lamination). Therefore, their growth is only constrained by contemporary dynamic factors, such as strain conditions. This reinforces the value of the study of magnetic fabric in remagnetized limestones (with low amounts of phyllosilicates) to characterize the tectonic setting under which this process occurs, either extensional or compressional (Sun et al., 1993; Calvín et al., submitted).

Applicability to basin evolution

New experiments to characterize the ferrimagnetic contribution in limestones, and the use of the partial restoration of the magnetic fabrics as shown here, could be useful in basins to understand if the magnetic lineation appearing in remagnetized limestones associated with RT-AMS prolate ellipsoids is related either to (i) paramagnetic minerals and extension during their deposition or, conversely, (ii) to remagnetization-carrier magnetite, following the stretching direction at remagnetization times. This can

give a picture of the tectonic setting under which the remagnetizations occurred in the different basins, and can shed light into some question not totally resolved at this time: e.g. are these remagnetization triggered by a change in the tectonic regime? Are the remagnetizations, and thus their associated AMS, synchronous? Which was the tectonic setting in the different basins during the post-rift stage? And ultimately, are the Iberian remagnetizations related to the Cretaceous rotation?

In summary, we have shown the possibilities of the analysis of ferrimagnetic fabrics in sedimentary basins, either using AARM or RT-AMS, or both, in remagnetized limestones not containing significant amounts of phyllosilicates. The application of the partial bedding correction (restoring beds to the remagnetization time) technique, can offer a unique view of the tectonic context under which the remagnetizations happened. The magnetic lineation carried by the ferrimagnetic minerals is demonstrated to be a good indicator of the stretching direction at the remagnetization time.

CONCLUSIONS

The magnetic fabrics of the carbonates that crop out in the Central High Atlas are analysed in 53 sites. For this purpose, the RT-AMS is measured systematically and compared with sub-fabrics (LT-AMS and AARM) to enhance the paramagnetic and the ferromagnetic signal, respectively.

The studied rocks are affected by a basin-scale chemical remagnetization carried by SSD magnetite. This remagnetization has an inter-folding behaviour because it was acquired during the Cretaceous (*ca.* 100 Ma), between the Jurassic extension and the Cenozoic compression. By means of previously published paleomagnetic results, the attitude of beds at the remagnetization time (i.e. the paleodip) can be known. We present here a new procedure that consists in applying a partial restoration to the magnetic fabrics (i.e. to restore according to the paleo-dip); the comparison between fabrics before bedding correction (BBC), after partial bedding correction (APBC), and after total bedding correction (ATBC), has provided key clues to unravel the magnetic fabrics carried by these rocks.

Four types of magnetic fabrics have been differentiated according to their directional behaviour:

- Type 1 RT-AMS shows prolate ellipsoids, with a clustered NNW-SSE lineation that becomes horizontal APBC. RT-AMS is coincident with AARM but not with LT-AMS. Comparing different sites, the best grouping of magnetic anisotropy axes is reached after this partial bedding correction.
- Type 2 RT-AMS shows intermediate directional behaviour between AARM and LT-AMS, magnetic foliation approaching LT-AMS results, and the magnetic lineation similar to the one obtained by means of AARM.
- Type 3 RT-AMS is coincident with LT-AMS but not with AARM. The magnetic foliation is normal to bedding and the magnetic lineation is normal to the intersection lineation between cleavage and bedding.
- Type 4 RT-AMS is also coincident with LT-AMS, with the magnetic foliation parallel to cleavage and the magnetic lineation parallel to the intersection lineation.

Furthermore, magnetic properties were measured in specimens from the different groups to determine differences that separate the established types. No differences were observed in the hysteresis parameters (indicating similar ferromagnetic mineralogy) or in the bulk susceptibility. However, type 1 shows high values in susceptibility of the ARM and dependence on the frequency of the susceptibility, indicating that this group presents more ferromagnetic minerals than the others in both magnetic states, SSD and SP magnetite. Therefore, we conclude that type 1 RT-AMS fabrics are carried by SP magnetite, with the same orientation than the SSD magnetite that carries the Cretaceous remagnetization and the AARM. This fabric is interpreted as extensional, showing the stretching at the remagnetization time. Type 3 and 4 RT-AMS fabrics are compressive fabrics, carried by phyllosilicates,

with different degrees of deformation. Finally, type 2 is an intermediate member between the extensional ferromagnetic fabric and the compressional paramagnetic fabric.

The last remarkable point is the difference in the response of magnetite and phyllosilicates to compression in the CHA. Magnetite grains are not affected by compression and thus they are capable to record an extensional secondary magnetic fabric fixed during the growth of the authigenic magnetite grains, whereas paramagnetic fabrics carried by phyllosilicates record secondary, compressional fabrics.

ACKNOWLEDGMENTS

AMS plots and κ-T curves have been analyzed with Anisoft 42 (Chadima and Jelinek, 2009) and Cureval 8.0 software (Chadima and Hrouda, 2009). Warm thanks to B Moussaid for help with field work. This study was funded by the MINECO (Spanish Ministry of Economy and Competitiveness) cofinanced by the ERDF (European Union) (research projects CGL2012-38481 and CGL2016-77560). PC acknowledges the MINECO (F.P.I. research grant BES-2013-062988). The authors sincerely thank the reviewers Bjarne Almqvist and Pedro Silva for their carefully and constructive comments, which have helped to improve the original manuscript. Raw ASM data can be found in the repository.

REFERENCES

Ait-Brahim, L., Chotin, P., Hinaj, S., Abdelouafi, A., El Adraoui, A., Nakcha, C., Dhont, D., Charroud, M., Sossey Alaoui, F., Amrhar, M., Bouaza, A., Tabyaoui, H., Chaouni, A., 2002. Paleostress evolution in the Moroccan African margin from Triassic to Present. Tectonophysics 357, 187–205. doi:10.1016/S0040-1951(02)00368-2

Armando, G., 1999. Intracontinental alkaline magmatism: Geology, Petrography, Mineralogy and Geochemistry of the Jebel Hayim Massif (Central High Atlas-Morocco). Mémories de Géologie de l'Université de Lausanne 31, 106.

Aubourg, C., Klootwijk, C., Korsch, R.J., 2004. Magnetic fabric constraints on oroclinal bending of the Texas and Coffs Harbour blocks: New England Orogen, eastern Australia. Geol. Soc. London, Spec. Publ. 238, 421–445. doi:10.1144/GSL.SP.2004.238.01.22

Aubourg, C., Smith, B., Eshraghi, A., Lacombe, O., Authemayou, C., Amrouch, K., Bellier, O., Mouthereau, F., 2010. New magnetic fabric data and their comparison with palaeostress markers in the Western Fars Arc (Zagros, Iran): tectonic implications. Geol. Soc. London, Spec. Publ. 330, 97–120. doi:10.1144/SP330.6

Banerjee, S., Elmore, R.D., Engel, M.H., 1997. Chemical remagnetization and burial diagenesis: Testing the hypothesis in the Pennsylvanian Belden Formation, Colorado. J. Geophys. Res. Solid Earth 102, 24825–24842. doi:10.1029/97JB01893

Bensalah, M.K., Youbi, N., Mata, J., Madeira, J., Martins, L., El Hachimi, H., Bertrand, H., Marzoli, A., Bellieni, G., Doblas, M., Font, E., Medina, F., Mahmoudi, A., Beraâouz, E.H., Miranda, R., Verati, C., De Min, A., Ben Abbou, M., Zayane, R., 2013. The Jurassic–Cretaceous basaltic magmatism of the Oued El-Abid syncline (High Atlas, Morocco): Physical volcanology, geochemistry and geodynamic implications. J. African Earth Sci. 81, 60–81. doi:10.1016/j.jafrearsci.2013.01.004

Bilardello, D., Jackson, M.J., 2014. A comparative study of magnetic anisotropy measurement techniques in relation to rock-magnetic properties. Tectonophysics 629, 39–54. doi:10.1016/j.tecto.2014.01.026

Blumstein, A.M., Elmore, R.D., Engel, M.H., Elliot, C., Basu, A., 2004. Paleomagnetic dating of burial diagenesis in Mississippian carbonates, Utah. J. Geophys. Res. 109, 1–16.

Borradaile, G.J., Hamilton, T., 2004. Magnetic fabrics may proxy as neotectonic stress trajectories, Polis rift, Cyprus. Tectonics 23, 278–7407.

Borradaile, G.J., Tarling, D.H., 1981. The influence of deformation mechanisms on magnetic fabrics in weakly deformed rocks. Tectonophysics 77, 151–168.

Borradaile, G.J., 1988. Magnetic susceptibility, petrofabrics and strain. Tectonophysics 156, 1–20. doi:10.1016/0040-1951(88)90279-X

Calvín, P., Casas-Sainz, A.M., Villalaín, J.J., Moussaid, B., 2018. Extensional vs. compressional deformation in the Central High Atlas salt province: A paleomagnetic approach. Tectonophysics 734–735, 130–147. https://doi.org/10.1016/j.tecto.2018.04.007

Calvín, P., Casas-Sainz, A.M., Villalaín, J.J., Moussaid, B., 2017a. Diachronous folding and cleavage in an intraplate setting (Central High Atlas, Morocco) determined through the study of remagnetizations. J. Struct. Geol. 97, 144–160. doi:10.1016/j.jsg.2017.02.009

Calvín, P., Ruiz-Martínez, V.C., Villalaín, J.J., Casas-Sainz, A.M., Moussaid, B., 2017b. Emplacement and Deformation of Mesozoic Gabbros of the High Atlas (Morocco): Paleomagnetism and Magnetic Fabrics. Tectonics. doi:10.1002/2017TC004578

Calvín, P., Villalaín, J.J., Casas-Sainz, A.M., Tauxe, L., Torres-López, S., 2017c. pySCu: a new python code for analyzing remagnetizations directions by means of Small Circle utilities. Comput. Geosci. 109. doi:10.1016/j.cageo.2017.07.002

Calvín, P., Villalaín, J.J., Casas-Sainz, A.M. Anisotropic magnetite growth in remagnetized limestones. Tectonic constraints and implications in basin history. Geology. submitted.

Caricchi, C., Cifelli, F., Kissel, C., Sagnotti, L., Mattei, M., 2016. Distinct magnetic fabric in weakly deformed sediments from extensional basins and fold-and-thrust structures in the Northern Apennine orogenic belt (Italy). Tectonics 35, 238–256. doi:10.1002/2015TC003940

Chadima, M., Hansen, A., Hirt, A.M., Hrouda, F., Siemes, H., 2004. Phyllosilicate preferred orientation as a control of magnetic fabric: evidence from neutron texture goniometry and low and high-field magnetic anisotropy (SE Rhenohercynian Zone of Bohemian Massif). Geol. Soc. London, Spec. Publ. 238, 361–380. doi:10.1144/GSL.SP.2004.238.01.19

Chadima, M., Hrouda, F., 2009. Cureval 8.0: Thermomagnetic Curve Browser for Windows. Agico Inc., Brno.

Channell, J.E.T., McCabe, C., 1994. Comparison of magnetic hysteresis parameters of unremagnetized and remagnetized limestones. J. Geophys. Res. Solid Earth 99, 4613–4623. doi:10.1029/93JB02578

Cifelli, F., Mattei, M., Chadima, M., Lenser, S., Hirt, A.M., 2009. The magnetic fabric in "undeformed clays": AMS and neutron texture analyses from the Rif Chain (Morocco). Tectonophysics 466, 79–88. https://doi.org/10.1016/j.tecto.2008.08.008

Cifelli, F., Mattei, M., Chadima, M., Hirt, A., Hansen, A., 2005. The origin of tectonic lineation in extensional basins: Combined neutron texture and magnetic analyses on "undeformed" clays. Earth Planet. Sci. Lett. 235, 62–78. doi:10.1016/j.epsl.2005.02.042

Cifelli, F., Mattei, M., Hirt, A.M., Günther, A., 2004. The origin of tectonic fabrics in "undeformed" clays: The early stages of deformation in extensional sedimentary basins. Geophys. Res. Lett. 31. doi:10.1029/2004GL019609

Dearing, J.A., Hay, K.L., Baban, S.M.J., Huddleston, A.S., Wellington, E.M.H., Loveland, P.J., 1996. Magnetic susceptibility of soil: an evaluation of conflicting theories using a national data set. Geophys. J. Int. 127, 728–734. doi:10.1111/j.1365-246X.1996.tb04051.x

Dudzisz, K., Szaniawski, R., Michalski, K., Chadima, M., 2018. Rock magnetism and magnetic fabric of the Triassic rocks from the West Spitsbergen Fold-and-Thrust Belt and its foreland. Tectonophysics 728–729, 104–118. https://doi.org/10.1016/j.tecto.2018.02.007

Ferré, E.C., 2002. Theoretical models of intermediate and inverse AMS fabrics. Geophys. Res. Lett. 29, 1127. https://doi.org/10.1029/2001GL014367

Frizon de Lamotte, D., Zizi, M., Missenard, Y., Hadif, M., El Azzouzi, M., Maury, R.C., Charrière, A., Taki, Z., Benammi, M., Michard, A., Hafid, M., Azzouzi, M. El, Maury, R.C., Charrière, A., Taki, Z., Benammi, M., Michard, A., 2008. The Atlas System, in: Michard, A., Saddiqi, O., Chalouan, A., Lamotte, D. de F. (Eds.), Continental Evolution: The Geology of Morocco. Lecture Notes in Earth Sciences 116. Springer, Berlin, Heidelberg, pp. 133–202. doi:10.1007/978-3-540-77076-3_4

García-Lasanta, C., Casas-Sainz, A., Villalaín, J.J., Oliva-Urcia, B., Mochales, T., Speranza, F., 2017. Remagnetizations used to unravel large-scale fold kinematics: a case study in the Cameros basin (N Spain). Tectonics. doi:10.1002/2016TC004459

García-Lasanta, C., Román-Berdiel, T., Oliva-Urcia, B., Casas, A.M., Gil-Peña, I., Speranza, F., Mochales, T., 2015. Tethyan versus Iberian extension during the Cretaceous period in the eastern Iberian Peninsula: insights from magnetic fabrics. J. Geol. Soc. London. 2015–68. doi:10.1144/jgs2015-068

García-Lasanta, C., Oliva-Urcia, B., Román-Berdiel, T., Casas, A.M.A.M., Hirt, A.M.A.M., 2014. Understanding the Mesozoic kinematic evolution in the Cameros basin (Iberian Range, NE Spain) from magnetic subfabrics and mesostructures. J. Struct. Geol. 66, 84–101. doi:10.1016/j.jsg.2014.05.013

Girdler, R.W., 1961. The Measurement and Computation of Anisotropy of Magnetic Susceptibility of Rocks. Geophys. J. Int. 5, 34–44. doi:10.1111/j.1365-246X.1961.tb02927.x

Gomez, F., Beauchamp, W., Barazangi, M., 2000. Role of the Atlas Mountains (northwest Africa) within the African-Eurasian plate-boundary zone. Geology 28, 775. doi:10.1130/0091-7613(2000)28<775:ROTAMN>2.0.CO;2

Graham, J.W., 1966. Significance of Magnetic Anisotropy in Appalachian Sedimentary Rocks, in: Steinhart, J.S., Smith, T.J. (Eds.), The Earth Beneath the Continents. American Geophysical Union, Geophysical Monograph Series, Washington, pp. 627–648. doi:10.1029/GM010p0627

Graham, J.W., 1954. Magnetic susceptibility anisotropy, an unexploited petrofabric element. Geol. Soc. Am. Bull. 65, 1257–1258.

Haddoumi, H., Charrière, A., Feist, M., Andreu, B., 2002. Nouvelles datations (Hauterivien supérieur-Barrémien inférieur) dans les «Couches rouges» continentales du Haut Atlas central marocain ; conséquences sur l'âge du magmatisme et des structurations mésozoïques de la chaîne Atlasique. Comptes Rendus - Palevol 1, 259–266. doi:10.1016/S1631-0683(02)00039-8

Hailwood, E. a., Mitchell, J.G., 1971. Palaeomagnetic and Radiometric Dating Results from Jurassic Intrusions in South Morocco. Geophys. J. Int. 24, 351–364. doi:10.1111/j.1365-246X.1971.tb02183.x

Hrouda, F., Jelínek, V., Zapletal, K., 1997. Refined technique for susceptibility resolution into ferromagnetic and paramagnetic components based on susceptibility temperature-variation measurement. Geophys. J. Int. 129, 715–719. https://doi.org/10.1111/j.1365-246X.1997.tb04506.x

Hrouda, F., 1994. A technique for the measurement of thermal changes of magnetic susceptibility of weakly magnetic rocks by the CS-2 apparatus and KLY-2 Kappabridge. Geophys. J. Int. 118, 604–612. https://doi.org/10.1111/j.1365-246X.1994.tb03987.x

Hrouda, F., Jelínek, V., 1990. Resolution of ferrimagnetic and paramagnetic anisotropies in rocks, using combined low-field and high-field measurements. Geophys. J. Int. 103, 75–84. https://doi.org/10.1111/j.1365-246X.1990.tb01753.x

Hrouda, F., 1982. Magnetic anisotropy of rocks and its application in geology and geophysics. Geophys. Surv. 5, 37–82. doi:10.1007/BF01450244

Issachar, R., Levi, T., Lyakhovsky, V., Marco, S., Weinberger, R., 2016. Improving themethod of low-temperature anisotropy of magnetic susceptibility (LT-AMS) measurements in air. Geochemistry, Geophys. Geosystems 2940–2950. doi:10.1002/2016GC006339.

Jackson, M.J., 1991. Anisotropy of magnetic remanence: A brief review of mineralogical sources, physical origins, and geological applications, and comparison with susceptibility anisotropy. Pure Appl. Geophys. PAGEOPH 136, 1–28. doi:10.1007/BF00878885

Jackson, M., Swanson-Hysell, N.L., 2012. Rock magnetism of remagnetized carbonate rocks: another look. Geol. Soc. London, Spec. Publ. 371, 229–251. doi:10.1144/sp371.3

Jelinek, V., 1981. Characterization of the magnetic fabric of rocks. Tectonophysics 79, T63–T67. doi:10.1016/0040-1951(81)90110-4

Kars, M., Aubourg, C., Labaume, P., Berquó, T., Cavailhes, T., 2014. Burial Diagenesis of Magnetic Minerals: New Insights from the Grès d'Annot Transect (SE France). Minerals 4, 667–689. https://doi.org/10.3390/min4030667

Katz, B., Elmore, R.D., Cogoini, M., Ferry, S., 1998. Widespread chemical remagnetization: orogenic fluids or burial diagenesis of clays? Geology 26, 603–606. doi:10.1130/0091-7613(1998)026<0603:WCROFO>2.3.CO

Kissel, C., Barrier, E., Laj, C., Lee, T.-Q., 1986. Magnetic fabric in "undeformed" marine clays from compressional zones. Tectonics 5, 769–781. doi:10.1029/TC005i005p00769

Lanci, L., Zanella, E., 2016. The anisotropy of magnetic susceptibility of uniaxial superparamagnetic particles: Consequences for its interpretation in magnetite and maghemite bearing rocks. J. Geophys. Res. B Solid Earth 121, 27–37. doi:10.1002/2015JB012255

Lee, T.-Q., Angelier, J., 2000. Tectonic significance of magnetic susceptibility fabrics in Plio-Quaternary mudstones of southwestern foothills, Taiwan. Earth, Planets Sp. 52, 527–538. https://doi.org/10.1186/BF03351660

Martín-Hernández, F., Ferré, E.C., 2007. Separation of paramagnetic and ferrimagnetic anisotropies: A review. J. Geophys. Res. Solid Earth 112. doi:10.1029/2006JB004340

Mattauer, M., Tapponnier, P., Proust, F., 1977. Sur les mecanismes de formation des chaines intracontinentales; l'exemple des chaines atlasiques du Maroc. Bull. la Soc. Geol. Fr. S7–XIX, 521–526. doi:10.2113/gssgfbull.S7-XIX.3.521

Mattei, M., Sagnotti, L., Faccenna, C., Funiciello, R., 1997. Magnetic fabric of weakly deformed clay-rich sediments in the Italian peninsula: Relationship with compressional and extensional tectonics. Tectonophysics 271, 107–122. doi:10.1016/S0040-1951(96)00244-2

Mattei, M., Speranza, F., Argentieri, A., Rossetti, F., Sagnotti, L., Funiciello, R., 1999. Extensional tectonics in the Amatea basin (Calabria, Italy) : a comparison between structural and magnetic anisotropy data. Tectonophysics 307, 33–49.

McCabe, C., Elmore, R.D., 1989. The occurrence and origin of Late Paleozoic remagnetization in the sedimentary rocks of North America. Rev. Geophys. 27, 471–494. doi:10.1029/RG027i004p00471

McCabe, C., Jackson, M., Ellwood, B.B., 1985. Magnetic anisotropy in the Trenton Limestone: Results of a new technique, anisotropy of anhysteretic susceptibility. Geophys. Res. Lett. 12, 333–336. doi:10.1029/GL012i006p00333

Michard, A., Ibouh, H., Charrière, A., 2011. Syncline-topped anticlinal ridges from the High Atlas: A Moroccan conundrum, and inspiring structures from the Syrian Arc, Israel. Terra Nov. 23, 314–323. doi:10.1111/j.1365-3121.2011.01016.x

Moskowitz, B.M., Jackson, M., Kissel, C., Moskowitz B.M., J.M.K.C., Moskowitz, B.M., Jackson, M., Kissel, C., 1998. Low-temperature magnetic behavior of titanomagnetites. Earth Planet. Sci. Lett. 157, 141–149. doi:10.1016/S0012-821X(98)00033-8

Moussaid, B., El Ouardi, H., Casas-Sainz, A., Villalaín, J.J., Román-Berdiel, T., Oliva-Urcia, B., Soto, R., Torres-López, S., 2013. Magnetic fabrics in the Jurassic–Cretaceous continental basins of the northern part of the Central High Atlas (Morocco): Geodynamic implications. J. African Earth Sci. 87, 13–32. doi:10.1016/j.jafrearsci.2013.07.001

Moussaid, B., Villalaín, J.J., Casas-Sainz, A., El Ouardi, H., Oliva-Urcia, B., Soto, R., Román-Berdiel, T., Torres-López, S., 2015. Primary vs. secondary curved fold axes: Deciphering the origin of the Aït Attab syncline (Moroccan High Atlas) using paleomagnetic data. J. Struct. Geol. 70, 65–77. doi:10.1016/j.jsg.2014.11.004

Nagata, T., 1961. Rock magnetism, 2nd editio. ed. Maruzen, Tokyo.

Oliva-Urcia, B., Gil-Peña, I., Soto, R., Samsó, J.M., Antolín, B., Pueyo, E.L., 2018. New insights into asymmetric folding by means of the anisotropy of magnetic susceptibility, Variscan and Pyrenean folds (SW Pyrenees). Stud. Geophys. Geod. 62. https://doi.org/10.1007/s11200-017-0143-6

Oliva-Urcia, B., Casas, A.M., Moussaid, B., Villalaín, J.J., El Ouardi, H., Soto, R., Torres-López, S., Román-Berdiel, T., 2016. Tectonic fabrics vs. mineralogical artifacts in AMS analysis: A case study

of the Western Morocco extensional Triassic basins. J. Geodyn. 94–95, 13–33. doi:10.1016/j.jog.2016.01.004

Oliva-Urcia, B., Casas, a. M., Ramón, M.J., Leiss, B., Mariani, E., Román-Berdiel, T., 2012. On the reliability of AMS in ilmenite-type granites: An insight from the Marimanha pluton, central Pyrenees. Geophys. J. Int. 189, 187–203. doi:10.1111/j.1365-246X.2011.05355.x

Oliva-Urcia, B., Casas, A.M., Soto, R., Villalaín, J.J., Kodama, K., 2011. A transtensional basin model for the Organyà basin (central southern Pyrenees) based on magnetic fabric and brittle structures. Geophys. J. Int. 184, 111–130. doi:10.1111/j.1365-246X.2010.04865.x

Oliva-Urcia, B., Larrasoaña, J.C., Pueyo, E.L., Gil, a., Mata, P., Parés, J.M., Schleicher, a. M., Pueyo, O., 2009. Disentangling magnetic subfabrics and their link to deformation processes in cleaved sedimentary rocks from the Internal Sierras (west central Pyrenees, Spain). J. Struct. Geol. 31, 163–176. doi:10.1016/j.jsg.2008.11.002

Özdemir, Ö., Dunlop, D.J., Moskowitz, B.M., 1993. The effect of oxidation on the Verwey transition in magnetite. Geophys. Res. Lett. 20, 1671–1674. https://doi.org/10.1029/93GL01483

Parés, J.M., 2015. Sixty years of anisotropy of magnetic susceptibility in deformed sedimentary rocks. Front. Earth Sci. 3, 1–13. doi:10.3389/feart.2015.00004

Parés, J.M., 2004. How deformed are weakly deformed mudrocks? Insights from magnetic anisotropy. Geol. Soc. London, Spec. Publ. 238, 191–203. doi:10.1144/GSL.SP.2004.238.01.13

Parés, J.M., van der Pluijm, B. a., 2014. Low-temperature AMS and the quantification of subfabrics in deformed rocks. Tectonophysics 629, 55–62. doi:10.1016/j.tecto.2014.03.005

Parés, J.M., van der Pluijm, B.A., Dinarès-Turell, J., 1999. Evolution of magnetic fabrics during incipient deformation of mudrocks (Pyrenees, northern Spain). Tectonophysics 307, 1–14. doi:10.1016/S0040-1951(99)00115-8

Parés, J.M., van der Pluijm, B.A., 2002. Phyllosilicate fabric characterization by Low-Temperature Anisotropy of Magnetic Susceptibility (LT-AMS). Geophys. Res. Lett. 29, 68-1-68–4. doi:10.1029/2002GL015459

Potter, D.K., 2004. A comparison of anisotropy of magnetic remanence methods - a user's guide for application to palaeomagnetism and magnetic fabric studies, in: Martin-Hernández, F., Lüneburg, C.M., Aubourg, C., Jackson, M. (Eds.), Magnetic Fabric: Methods and Applications, Geological Society Special Publications. The Geological Society of London, London, pp. 21–36. doi:10.1144/GSL.SP.2004.238.01.03

Potter, D.K., Stephenson, A., 1988. Single-domain particles in rocks and magnetic fabric analysis. Geophys. Res. Lett. 15, 1097–1100. doi:10.1029/GL015i010p01097

Pueyo Anchuela, Ó., Gil Imaz, A., Pocoví Juan, A., 2010. Significance of AMS in multilayer systems in fold-and-thrust belts. A case study from the Eocene turbidites in the Southern Pyrenees (Spain). Geol. J. 45, 544–561. doi:10.1002/gj.1194

Pueyo Anchuela, Ó., María Casas-Sainz, A., Pocoví Juan, A., Gil Imaz, A., 2011. Lithology-dependent reliability of AMS analysis: A case study of the Eocene turbidities in the southern Pyrenees (Aragón, Spain). Comptes Rendus Geosci. 343, 11–19. doi:10.1016/j.crte.2010.11.003

Radhakrishnamurty, C., Likhite, S.D., 1993. Frequency dependence of low-temperature susceptibility peak in some titanomagnetites. Phys. Earth Planet. Inter. 76, 131–135.

Richter, C., van der Pluijm, B.A., 1994. Separation of paramagnetic and ferrimagnetic susceptibilities using low temperature magnetic susceptibilities and comparison with high field methods. Phys. Earth Planet. Inter. 82, 111–121.

Rochette, P., Jackson, M., Aubourg, C., 1992. Rock magnetism and the interpretation of anisotropy of magnetic susceptibility. Rev. Geophys. 30, 209–226. doi:10.1029/92RG00733

Rochette, P., Fillion, G., 1988. Identification of multicomponent anisotropies in rocks using various field and temperature values in a cryogenic magnetometer. Phys. Earth Planet. Inter. 51, 379–386. https://doi.org/10.1016/0031-9201(88)90079-9

Rochette, P., 1987. Magnetic susceptibility of the rock matrix related to magnetic fabric studies. J. Struct. Geol. 9, 1015–1020. doi:10.1016/0191-8141(87)90009-5

Sagnotti, L., Speranza, F., Winkler, A., Mattei, M., Funiciello, R., 1998. Magnetic fabric of clay sediments from the external northern Apennines (Italy). Phys. Earth Planet. Inter. 105, 73–93.

Santolaria, P., Casas, A.M., Soto, R., 2015. Anisotropy of magnetic susceptibility as a proxy to assess internal deformation in diapirs: case study of the Naval salt wall (Southern Pyrenees). Geophys. J. Int. 202, 1207–1222. doi:10.1093/gji/ggv231

Schmidt, V., Hirt, A.M., Leiss, B., Burlini, L., Walter, J.M., 2009. Quantitative correlation of texture and magnetic anisotropy of compacted calcite–muscovite aggregates. J. Struct. Geol. 31, 1062–1073. https://doi.org/10.1016/j.jsg.2008.11.012

Schmidt, V., Hirt, A.M., Rosselli, P., Martín-Hernández, F., 2007. Separation of diamagnetic and paramagnetic anisotropy by high-field, low-temperature torque measurements. Geophys. J. Int. 168, 40–47. https://doi.org/10.1111/j.1365-246X.2006.03202.x

Soto, R., Beamud, E., Roca, E., Carola, E., Almar, Y., 2017. Distinguishing the effect of diapir growth on magnetic fabrics of syn-diapiric overburden rocks: Basque-Cantabrian basin, Northern Spain. Terra Nov. 38, 42–49. doi:10.1111/ter.12262

Soto, R., Kullberg, J.C., Oliva-Urcia, B., Casas-Sainz, A.M., Villalaín, J.J., 2012. Switch of Mesozoic extensional tectonic style in the Lusitanian basin (Portugal): Insights from magnetic fabrics. Tectonophysics 536–537, 122–135. doi:10.1016/j.tecto.2012.03.010

Soto, R., Larrasoaña, J.C., Arlegui, L.E., Beamud, E., Oliva-Urcia, B., Simón, J.L., 2009. Reliability of magnetic fabric of weakly deformed mudrocks as a palaeostress indicator in compressive settings. J. Struct. Geol. 31, 512–522. doi:10.1016/j.jsg.2009.03.006

Soto, R., Villalaín, J.J., Casas-Sainz, A.M., 2008. Remagnetizations as a tool to analyze the tectonic history of inverted sedimentary basins: A case study from the Basque-Cantabrian basin (north Spain). Tectonics 27, n/a-n/a. doi:10.1029/2007TC002208

Stephenson, A., Sadikun, S., Potter, D.K., 1986. A theoretical and experimental comparison of the anisotropies of magnetic susceptibility and remanence in rocks and minerals. Geophys. J. R. Astron. Soc. 84, 185–200.

Suk, D.-W., der Voo, R., Peacor, D.R., 1993. Origin of magnetite responsible for remagnetization of early Paleozoic limestones of New York State. J. Geophys. Res. B Solid Earth 98, 419–434.

Suk, D., Peacor, D.R., Van Der Voo, R., 1990. Replacement of pyrite framboids by magnetite in limestone and implications for palaeomagnetism. Nature 345, 611–613.

Sun, W., Jackson, M., Craddock, J.P., 1993. Relationship between remagnetization, magnetic fabric and deformation in Paleozoic carbonates. Tectonophysics 221, 361–366. doi:10.1016/0040-1951(93)90167-I

Tarling, D.H., Hrouda, F., 1993. The Magnetic Anisotropy of Rocks. Chapman & Hall, London.

Torres-López, S., Villalaín, J.J., Casas, A.M., EL Ouardi, H., Moussaid, B., Ruiz-Martínez, V.C., 2014. Widespread Cretaceous secondary magnetization in the High Atlas (Morocco). A common origin for the Cretaceous remagnetizations in the western Tethys? J. Geol. Soc. London. 171, 673–687. doi:10.1144/jgs2013-107

Torres-López, S., Casas, A.M., Villalaín, J.J., El Ouardi, H., Moussaid, B., 2016. Pre-Cenomanian vs. Cenozoic folding in the High Atlas revealed by palaeomagnetic data. Terra Nov. 28, 110–119. doi:10.1111/ter.12197

Villalaín, J., Fernández-González, G., Casas, A.M., Gil-Imaz, A., 2003. Evidence of a Cretaceous remagnetization in the Cameros Basin (North Spain): implications for basin geometry. Tectonophysics 377, 101–117. doi:10.1016/j.tecto.2003.08.024

Villalaín, J.J., Casas-Sainz, A.M., Soto, R., 2016. Reconstruction of inverted sedimentary basins from syn-tectonic remagnetizations. A methodological proposal. Geol. Soc. London, Spec. Publ. 425, 233–246. doi:10.1144/SP425.10

Verwey, E.J., 1939. Electronic Conduction of Magnetite (Fe3O4) and its Transition Point at Low Temperatures. Nat. 144, 327–328. https://doi.org/10.1038/144327b0

Walz, F., 2002. The Verwey transition - a topical review. J. Phys. Condens. Matter 14, R285–R340. https://doi.org/10.1088/0953-8984/14/12/203

Worm, H.U., 1998. On the superparamagnetic-stable single domain transition for magnetite, and frequency dependence of susceptibility. Geophys. J. Int. 133, 201–206.

Worm, H.U., Jackson, M., 1999. The superparamagnetism of Yucca Mountain Tuff. J. Geophys. Res. B Solid Earth 104, 25,415-425,425.

Zayane, R., Essaifi, A., Maury, R.C., Piqué, A., Laville, E., Bouabdelli, M., 2002. Cristallisation fractionnée et contamination crustale dans la série magmatique jurassique transitionnelle du Haut Atlas central (Maroc). Comptes Rendus Geosci. 334, 97–104. doi:10.1016/S1631-0713(02)01716-9

Zhao, X., Liu, Q., 2010. Effects of the grain size distribution on the temperature-dependent magnetic susceptibility of magnetite nanoparticles. Sci. China Earth Sci. 53, 1071–1078. doi:10.1007/s11430-010-4015-y

FIGURE CAPTIONS

Figure 1. (a) Location of the Central High Atlas (CHA) in the westernmost Mediterranean area. Synthetic geological map of the CHA and location of the study area (Fig. 3). Modified after Teixell et al. (2003). (c) Cross-section of the study area.

Figure 2. Synthesis of the main geological events occurred in the CHA with noticeable imprint in the magnetic fabric and paleomagnetic directions of the studied sites (data from Calvín et al., 2017a). Equal-area projections with the small circles and the remagnetization site mean directions before bedding correction (BBC), after partial bedding correction (APBC) and after total bedding correction (ATBC) are also shown.

Figure 3. (a) Geological map of the study area showing the sites classified according to the observed type of RT-AMS. Lower hemisphere, equal area projections showing (b) the poles to bedding and (c) the paleo-bedding with their associated cylindrical best-fit and the density isolines, (d) the great circles and poles to cleavage and (e) the intersection lineation between bedding and cleavage.

Figure 4. Pictures of outcrops showing different attitudes and deformation degrees of the sampled limestones. Solid lines mark the bedding (S_0) and dashed lines the cleavage (S_1).

Figure 5. Thin-sections photomicrographs showing different aspects of deformational structures in the analysed limestones. AG02: bioclastic limestones without cleavage. SK14, SK05 and AM01: micritic limestones with contribution of detrital grains, with pressure-solution cleavage (S_1). SK01: bioclastic limestones with a well-defined pressure-solution cleavage with concentration of oxides (and probably

also phyllosilicates) in the cleavage surfaces. Note the presence in all samples of bedding-parallel pyrite grains showing framboidal morphologies in some cases (see the inset in SK01).

Figure 6. Lower hemisphere, equal area projection of the principal axes of (a) RT-AMS, (b) LT-AMS and (c) AARM, for all studied sites, showing the corrected anisotropy degree (P_j) versus bulk susceptibility (κ_{RT}) and shape parameter (T), as well. BBC: before bedding correction; APBC: after partial bedding correction; ATBC: after total bedding correction.

Figure 7. Equal-area projection of the different fabrics (RT-AMS, LT-AMS and AARM) for two selected sites representative of types (a) 1 and (b) 2 together with the corresponding P_j-T plot.

Figure 8. Equal area projection of the different fabrics (RT-AMS, LT-AMS and AARM) for two selected sites representative of types (a) 3 and T(b) 4 together with the corresponding P_j-T plot.

Figure 9. RT-AMS for all samples, classified according to the five different groups.

Figure 10. a) κ_{LT}/κ_{RT} ratio vs. κ_{RT} showing in different colours the different groups. b) Heating κ-T curves from liquid nitrogen temperature (~ -196 ºC) to 700 ºC, showing the paramagnetic fit calculated with the Cureval software (Chadima and Hrouda, 2009) following Hrouda (1994) and Hrouda et al. (1997); the calculated ferromagnetic (ferro) and paramagnetic (para) ratios are indicated. c) Equal area projection of the principal axes of the RT-AMS for site AM13, showing specimens with type 2 behaviour (-03 and -04) and the type 1 behaviour.

Figure 11. a) Hysteresis parameters plot and mixing curves for magnetite (Dunlop, 2002). Measured specimens are in the SP-SSD mixing zone, independently of the observed RT-AMS type. b-e) Box and

whisker plot showing the median and the quartiles of the different parameters measured in specimens. b) susceptibility of the ARM (χ_{ARM}). c) Bulk susceptibility at room temperature (κ_{RT}). d) Percentage of frequency-dependent susceptibility measured at room temperature ($\%\chi_{fd}$). e) Shape parameter (T) of the RT-AMS (white boxes) and AARM (grey boxes).

Fig. 12. Sketch showing the relationship between magnetic mineralogy, tectonic processes and observed RT-AMS. Type 1 is pure ferrimagnetic interpreted as related to extensional features whereas type 3 and 4 are paramagnetic fabrics related to compression. Type 2 shows intermediate attitudes, showing extensional and ferrimagnetic lineation and paramagnetic and compaction foliation. Compressional ferrimagnetic fabrics have not been observed in the study area.

Table 1. Location of the studied sites, type of ellipsoid defined by the RT-AMS, and scalar parameters of the RT-AMS. N/n: number of total data vs. number of used data; km: bulk susceptibility; L: magnetic lineation; F: magnetic foliation; P_j: corrected anisotropy degree; T: shape parameter; σ: standard deviation; U: unclassified type.

Site	Coordinates (WGS86)		Type of	N/n	km	σ	L	σ	F	σ	P_j	σ	T	σ
	Longitude	Latitude	ellipsoid		$X10^{-6}$ SI									
AG02	-5.4775792563	32.0222007889	1	7/7	756	459	1.022	0.008	1.01	0.005	1.033	0.01	-0.374	0.277
AM04	-5.0439580000	32.2736890000	1	12/12	619	176	1.023	0.006	1.007	0.003	1.031	0.005	-0.526	0.251
AM13	-4.9543220000	32.2719410000	1	12/12	603	331	1.009	0.004	1.012	0.007	1.022	0.006	0.076	0.434
AM14	-5.1019540000	32.2761530000	1	13/13	530	102	1.021	0.005	1.01	0.003	1.032	0.004	-0.335	0.211
DP01	-5.6653333333	32.1274666667	1	8/8	287	56.6	1.019	0.013	1.01	0.007	1.03	0.011	-0.178	0.636
DP02	-5.6653333333	32.1274666667	1	8/8	173	167	1.018	0.012	1.066	0.004	1.026	0.013	-0.38	0.49
DP05	-5.5874166667	32.1423666667	1	8/8	373	610	1.003	0.001	1.002	0.001	1.006	0.002	-0.166	0.347
DP06	-5.5888333333	32.1428415000	1	11/11	458	49	1.007	0.005	1.005	0.002	1.012	0.005	-0.057	0.53
DP10	-5.5987000000	32.1288333333	1	10/10	189	37.3	1.011	0.006	1.006	0.003	1.017	0.005	-0.22	0.488
OU02	-5.3680260000	32.1566960000	1	12/12	226	120	1.008	0.003	1.008	0.005	1.017	0.006	-0.016	0.38
OU03	-5.3710290000	32.1502090000	1	10/10	181	90.6	1.022	0.01	1.021	0.014	1.043	0.022	-0.058	0.263
OU06	-5.3220820000	32.1325970000	1	12/12	315	147	1.014	0.004	1.007	0.003	1.022	0.005	-0.361	0.219
SK05	-5.4682166667	32.0436165000	1	17/17	230	198	1.014	0.012	1.014	0.008	1.028	0.018	0.106	0.397
SK07	-5.4688000000	32.0386306667	1	13/13	1.72	40.6	1.01	0.006	1.013	0.014	1.024	0.013	-0.045	0.564
SK09	-5.4708093899	32.0326174154	1	7/7	790	169	1.029	0.01	1.01	0.003	1.041	0.011	-0.442	0.227
SK14	-5.3253166667	32.1482173333	1	12/12	478	142	1.015	0.005	1.007	0.004	1.024	0.004	-0.327	0.358
SK15	-5.3301000000	32.1434253000	1	11/11	169	31.7	1.007	0.004	1.008	0.003	1.016	0.003	0.102	0.422
SK19	-5.3801388333	32.1303691667	1	15/15	274	89	1.018	0.01	1.009	0.004	1.029	0.013	-0.263	0.305
AM06	-4.9612480000	32.2959210000	2	13/13	227	31	1.015	0.005	1.016	0.005	1.031	0.003	0.039	0.291
DP04	-5.6679666667	32.1295166667	2	7/7	197	32.8	1.006	0.003	1.016	0.007	1.023	0.006	0.411	0.389
OU04	-5.3701710000	32.1495530000	2	10/10	315	40.8	1.004	0.002	1.018	0.007	1.024	0.008	0.584	0.18
SK04	-5.4790333333	32.0758023333	2	12/12	124	256	1.005	0.004	1.018	0.009	1.025	0.012	0.577	0.25
SK12	-5.4748666667	31.9483000000	2	11/11	301	113	1.008	0.004	1.06	0.011	1.075	0.013	0.757	0.134
SK16	-5.2474666667	32.1355240000	2	7/7	479	159	1.015	0.007	1.011	0.005	1.026	0.008	-0.117	0.464
AM01	-5.0903890000	32.2135470000	3	7/7	323	110	1.015	0.004	1.019	0.006	1.035	0.006	0.137	0.247
AM02	-5.0537886044	32.2303715708	3	12/12	112	34.8	1.009	0.004	1.024	0.009	1.035	0.012	0.433	0.171
AM07	-4.7608470004	32.2683762996	3	13/13	234	49.9	1.005	0.002	1.016	0.002	1.023	0.003	0.543	0.17
AM12	-4.8198670000	32.2909960000	3	8/8	310	98.7	1.011	0.003	1.011	0.005	1.023	0.006	-0.068	0.388
AM16	-4.9743190000	32.2809610000	3	8/8	722	914	1.019	0.005	1.011	0.005	1.032	0.003	-0.27	0.322
DP03	-5.6653333333	32.1274666667	3	7/7	818	496	1.099	0.007	1.022	0.007	1.032	0.011	0.478	0.309
OU01	-5.3626490000	32.1470260000	3	8/8	372	51.3	1.008	0.005	1.01	0.002	1.019	0.004	0.18	0.349
OU07	-5.3044540000	32.1367200000	3	10/10	247	52.5	1.007	0.003	1.01	0.005	1.018	0.005	0.097	0.434
SK10	-5.5125000000	31.9963333333	3	6/6	167	142	1.019	0.014	1.007	0.004	1.028	0.017	-0.26	0.514
SK17	-5.2458833333	32.1371576667	3	7/7	323	97.3	1.018	0.011	1.023	0.012	1.043	0.016	0.145	0.416
AM05	-4.9305720000	32.3343230000	4	8/8	370	56	1.005	0.003	1.013	0.003	1.019	0.003	0.415	0.315
AM08	-4.8096290000	32.2655130000	4	10/10	197	26.4	1.014	0.003	1.038	0.004	1.055	0.006	0.458	0.102
AM09	-4.8208030000	32.2706410000	4	6/6	259	23	1.008	0.001	1.015	0.003	1.024	0.004	0.286	0.124
AM10	-4.8205335533	32.2708180885	4	3/3	253	15.6	1.005	0.004	1.013	0.004	1.02	0.006	0.439	0.267
AM11	-4.8207239530	32.2709996914	4	5/5	283	12.3	1.004	0.002	1.004	0.002	1.008	0.002	-0.087	0.436
OU05	-5.3701360000	32.1477500000	4	8/4	336	55	1.009	0.003	1.012	0.004	1.021	0.006	0.136	0.165
SK01	-5.5812961667	32.1510336667	4	10/10	171	47	1.006	0.002	1.025	0.018	1.033	0.021	0.558	0.16
SK06	-5.4695500000	32.0398310000	4	6/6	189	44.8	1.011	0.004	1.014	0.007	1.025	0.011	0.104	0.237
SK08	-5.4708479598	32.0328691962	4	6/6	334	68.8	1.015	0.003	1.006	0.002	1.022	0.003	-0.409	0.171
SK11	-5.5137666667	31.9958123333	4	7/7	584	57.5	1.027	0.013	1.016	0.01	1.044	0.016	-0.28	0.339
AG01	-5.4775860517	32.0223116547	U	13/12	164	48.7	1.005	0.003	1.01	0.006	1.016	0.007	0.186	0.403
AM03	-5.0290900000	32.2349690000	U	12/12	513	107	1.012	0.004	1.007	0.003	1.019	0.005	-0.293	0.235
AM15	-5.0567310000	32.3029890000	U	8/8	344	197	1.006	0.001	1.003	0.001	1.009	0	-0.315	0.155
DP07	-5.5909000000	32.1534241667	U	6/6	139	21.3	1.01	0.004	1.024	0.007	1.036	0.007	0.385	0.263
DP08	-5.5902166667	32.1256740000	U	4/4	150	10.2	1.02	0.006	1.028	0.008	1.049	0.005	0.159	0.281
DP09	-5.5948833333	32.1251833333	U	8/8	240	33.7	1.027	0.015	1.019	0.012	1.048	0.024	-0.19	0.338
DP11	-5.6015666667	32.1289411667	U	8/8	99.7	41.2	1.023	0.013	1.011	0.006	1.036	0.016	-0.34	0.278
SK13	-5.4719666667	32.0284786667	U	7/7	811	282	1.012	0.01	1.015	0.011	1.028	0.014	0.099	0.589
SK18	-5.3846790000	32.1373333333	U	8/8	555	117	1.01	0.004	1.009	0.005	1.02	0.005	-0.067	0.348

Table 2. Structural and RT-AMS directional data. Bedding, paleo-bedding and cleavage, as dip direction and dip of the maximum dip direction; L_1 (lineation of intersection) as trend and plunge (calculated from bedding and cleavage data). Principal axis of the RT-AMS direction are given as trend and plunge before bedding correction (BBC), after partial bedding correction (APBC) and after total bedding correction (ATBC), with the corresponding angles of confidence (e1 and e2); U: unclassified type.

Site	Bedding	Paleo-Bedding	Cleavage	L_1	Type of ellipsoid	kmax				kint				kmin			
						BBC	APBC	ATBC	e1/e2	BBC	APBC	ATBC	e1/e2	BBC	APBC	ATBC	e1/e2
AG02	001/00	001/02	-/-	-/-	1	340/08	340/08	340/07	19/2	072/14	072/14	072/14	35/15	223/74	223/74	225/75	33/3
AM04	191/22	191/22	208/72	201/22	1	160/14	160/14	341/05	8/4	070/02	070/02	072/13	12/8	331/76	331/76	232/76	11/4
AM13	148/34	148/20	-/-	-/-	1	167/22	166/09	345/10	8/6	076/02	256/01	254/08	33/6	341/68	355/81	126/77	34/3
AM14	353/46	353/09	-/-	-/-	1	332/32	155/03	155/12	14/5	064/02	246/10	248/12	27/10	157/58	048/80	023/73	26/4
DP01	355/71	175/07	-/-	-/-	1	323/68	163/07	344/00	15/12	077/09	254/06	254/05	35/12	170/20	025/81	075/85	35/15
DP02	350/60	350/04	-/-	-/-	1	330/52	158/03	158/07	9/7	067/05	248/08	249/09	62/7	161/38	049/82	030/79	62/8
DP05	293/87	293/79	-/-	-/-	1	007/20	005/17	182/14	12/6	257/45	261/38	083/32	40/10	114/39	114/47	392/54	40/6
DP06	303/59	303/46	-/-	-/-	1	141/07	142/20	162/61	19/9	234/22	238/17	062/05	29/7	033/67	006/64	330/38	28/9
DP10	333/71	333/74	-/-	-/-	1	158/23	158/20	284/84	31/6	067/02	068/02	062/05	35/17	332/67	332/70	153/04	26/10
OU02	298/39	298/04	-/-	-/-	1	318/23	136/10	137/14	57/10	225/05	045/05	045/07	57/21	123/66	287/79	290/75	21/9
OU03	314/64	314/58	-/-	-/-	1	321/09	321/03	145/55	17/7	132/81	128/87	314/35	19/14	230/01	230/01	048/05	16/6
OU06	188/15	188/03	192/78	102/01	1	186/08	007/04	007/07	29/9	279/19	275/19	274/18	29/18	075/70	109/71	117/70	18/8
SK05	333/48	333/26	163/70	250/08	1	324/17	144/05	143/31	13/12	056/07	054/04	233/00	16/9	169/72	285/83	323/59	14/12
SK07	160/14	160/05	-/-	-/-	1	163/09	163/00	343/05	14/6	073/01	071/00	253/00	12/9	339/81	318/90	162/85	11/8
SK09	180/16	180/04	-/-	-/-	1	178/01	358/11	358/15	8/4	087/17	091/18	092/17	25/6	270/73	237/69	229/67	25/5
SK14	180/64	180/38	192/55	248/39	1	170/32	171/08	350/31	8/6	263/04	262/01	083/05	19/8	358/58	356/82	182/58	19/6
SK15	202/41	202/21	290/41	246/32	1	159/20	162/05	341/11	14/6	259/27	253/15	250/02	25/12	038/56	055/74	152/79	24/7
SK19	177/28	177/20	330/85	241/13	1	150/12	150/05	329/13	8/6	308/77	269/81	204/68	24/7	059/05	059/08	064/17	24/7
AM06	134/32	134/08	182/85	294/26	2	143/30	142/06	322/02	7/4	051/04	052/01	232/01	7/6	315/60	317/84	123/88	6/4
DP04	355/14	175/06	-/-	-/-	2	329/11	329/04	149/02	21/7	061/11	060/08	059/05	21/6	196/74	214/81	256/84	11/4
OU04	129/110	129/96	-/-	-/-	2	313/59	316/73	127/11	31/6	197/15	195/09	032/25	31/5	100/27	102/14	238/62	6/4
SK04	015/20	015/05	088/45	020/20	2	298/8	300/04	300/03	21/7	031/20	030/05	030/00	22/6	188/69	172/83	128/87	9/6
SK12	018/01	018/05	-/-	-/-	2	005/02	005/01	005/01	45/5	095/01	095/01	095/01	45/3	202/88	227/89	227/89	5/3
SK16	318/18	138/01	-/-	-/-	2	298/17	299/02	299/00	15/9	208/00	208/06	209/07	19/15	117/73	047/84	029/84	19/10
AM01	004/17	004/22	003/50	093/00	3	117/07	118/05	114/13	13/4	209/13	208/09	212/29	12/7	000/75	358/80	002/58	9/7
AM02	175/60	175/24	010/60	092/13	3	095/26	109/15	112/04	15/8	233/57	208/31	203/10	16/12	356/19	357/55	360/79	14/6
AM07	318/26	318/13	175/87	264/16	3	258/06	079/01	078/07	40/8	349/07	169/04	170/15	40/3	129/81	340/86	323/73	8/4
AM12	338/24	338/8	005/85	276/12	3	315/19	316/05	136/03	18/7	049/11	047/05	046/02	18/4	167/68	186/83	278/86	7/4
AM16	155/36	155/21	-/-	-/-	3	209/18	206/09	026/05	12/6	115/12	116/00	295/16	15/7	354/69	26/81	131/73	15/11
DP03	001/25	181/04	-/-	-/-	3	065/11	243/03	242/01	13/2	034/20	152/06	152/03	14/4	183/67	356/84	346/88	7/3
OU01	228/30	228/46	138/60	210/29	3	247/48	256/63	241/19	20/8	341/05	162/02	336/15	21/6	075/42	071/27	103/65	10/7
OU07	160/80	160/57	187/89	100/70	3	112/52	130/37	140/01	16/5	230/20	225/07	050/19	26/13	333/31	325/52	232/71	25/4
SK10	320/59	320/9	113/74	031/28	3	042/12	039/08	037/06	10/9	311/07	131/14	130/23	15/10	192/76	279/74	293/66	15/9
SK17	143/55	143/06	-/-	-/-	3	062/12	068/01	248/01	20/7	162/38	338/09	338/15	20/10	318/49	164/81	338/15	10/7
AM05	334/55	334/04	320/50	291/46	4	035/18	212/10	212/12	38/12	392/35	120/07	120/10	38/10	147/50	356/78	351/75	14/8
AM08	150/52	150/49	337/87	066/08	4	311/72	074/30	092/10	12/8	239/58	234/58	188/31	11/4	338/06	339/09	346/57	10/3
AM09	315/13	135/02	178/67	265/08	4	127/43	126/54	125/56	16/6	260/36	266/29	267/28	17/8	011/26	007/19	006/18	8/6
AM10	288/34	288/31	167/79	27/246	4	-/-	-/-	-/-	-/-	-/-	-/-	-/-	-/-	-/-	-/-	-/-	-/-
AM11	193/53	193/47	338/75	257/30	4	075/34	049/37	120/41	67/10	296/48	290/49	246/35	67/12	181/21	181/16	360/30	16/6
OU05	223/40	223/83	305/80	224/40	4	-/-	-/-	-/-	-/-	-/-	-/-	-/-	-/-	-/-	-/-	-/-	-/-
SK01	103/61	103/60	116/75	038/37	4	032/25	033/24	224/03	28/6	169/58	167/57	133/13	28/8	293/20	293/21	328/77	9/5
SK06	160/72	160/14	338/58	249/02	4	067/09	076/07	077/	19/9	252/81	170/32	169/18	28/14	157/01	335/57	331/71	27/15
SK08	158/49	158/08	340/65	069/01	4	088/04	266/09	264/12	34/26	178/01	003/37	006/44	72/29	281/86	164/51	163/43	72/26
SK11	338/74	338/04	145/80	066/09	4	058/22	224/02	224/03	14/9	152/09	128/77	115/81	27/11	263/66	315/13	315/09	26/8
AG01	344/68	344/31	334/83	060/31	U	068/04	067/00	248/04	53/22	336/28	157/09	155/39	53/32	166/62	337/81	342/50	34/18
AM03	170/53	170/31	178/89	088/10	U	329/28	321/48	282/70	12/5	159/62	163/40	165/10	34/11	061/04	064/11	072/18	34/6
AM15	285/22	285/02	180/89	270/21	U	174/03	176/10	177/11	8/4	079/58	051/73	045/75	9/7	266/32	269/13	269/11	9/5
DP07	325/70	325/09	-/-	-/-	U	018/04	211/30	216/33	77/16	285/34	112/16	110/24	77/3	113/56	357/55	351/47	17/6
DP08	138/82	138/73	-/-	-/-	U	-/-	-/-	-/-	-/-	-/-	-/-	-/-	-/-	-/-	-/-	-/-	-/-
DP09	124/78	124/58	-/-	-/-	U	144/19	143/01	337/53	48/19	249/37	234/46	177/35	55/25	032/47	053/44	080/10	45/19
DP11	305/51	305/51	-/-	-/-	U	186/26	186/26	220/38	48/26	090/12	090/12	067/49	48/38	338/60	338/61	321/13	41/21
SK13	013/62	016/22	168/44	094/16	U	329/01	142/27	130/39	43/18	239/27	266/48	292/50	45/17	061/63	036/29	033/09	27/18
SK18	171/55	171/60	165/80	253/11	U	279/23	282/22	251/28	25/14	170/38	170/43	351/17	21/14	034/43	031/40	005/56	21/12

Ferromagnetic fabrics carried by authigenic superparamagnetic magnetite
Ferromagnetic fabrics can be interpreted in terms of strain conditions during remagnetization
Paramagnetic fabrics record the Cenozoic compression whereas the ferromagnetic ones record the extension
Novel partial restoration approach of the magnetic fabric to the time of magnetite growth